ADVANCED FUNCTIONAL MATERIALS
www.afm-journal.de

Enhancing Field-Effect Mobility of Conjugated Polymers Through Rational Design of Branched Side Chains

*Boyi Fu, Jose Baltazar, Ashwin Ravi Sankar, Ping-Hsun Chu, Siyuan Zhang, David M. Collard, and Elsa Reichmanis**

The design of polymer semiconductors possessing effective π–π intermolecular interactions coupled with good solution processability remains a challenge. Structure-property relationships associated with side chain structure, π–π intermolecular interactions, polymer solubility, and charge carrier transport are reported for a donor–acceptor(1)-donor–acceptor(2) polymer: 5-Decylheptadecyl (5-DH), 2-tetradecyl (2-DT), and linear n-octadecyl (OD) chains are substituted onto a polymer backbone consisting of terthiophene units (T) between two different electron acceptors, benzothiadiazole (B), and diketopyrrolopyrrole (D), pTBTD, to afford pTBTD-5DH, pTBTD-2DT, and pTBTD-OD, respectively. In the 5-DH side chain, the branching position is remote from the polymer backbone, whereas it is proximal in 2-DT. This study demonstrates that incorporation of branched side chains where the branching position is remote from the polymer backbone merges the advantages of improved solubility from branched units with effective π–π intermolecular interactions normally associated with linear chains on conjugated polymers. pTBTD-5DH exhibits superior qualities with respect to the degree of polymerization, solution processability, π–π interchain stacking, and charge carrier transport relative to the other analogs. pTBTD-5DH exhibits a field-effect hole mobility of up to 2.95 $cm^2 V^{-1} s^{-1}$, a factor of 3–7 times that achieved with pBDT6-DT and pBDT6-OD.

1. Introduction

Side chain engineering has a significant potential to aid the development of high performance semiconducting π-conjugated polymers for optoelectronic applications.[1–3] Optimization of the solution processability and intermolecular interactions in thin films of these materials is important in the design of new polymeric semiconductors.[4,5] Here we describe the influence of the structure of side chains on the solubility and interchain interactions that govern charge carrier transport in a new low bandgap polymer.

We recently introduced poly(benzothiadiazole-*alt*-sexithiophene), **pBT6**, a polymeric semiconductor composed of alternating benzothiadiazole (acceptor) and sexithiophene (donor) units with *n*-dodecyl side chains to impart solubility. It displays a bandgap of 1.5 eV and a hole mobility of up to 0.75 $cm^2 V^{-1} s^{-1}$.[6] To further enhance the semiconducting performance of this class of materials, we incorporated diketopyrrolopyrrole units as a second acceptor into the structure of **pBT6**. The new polymer consists of electron-donating terthiophene units (**T**) between two different electron acceptors, benzothiadiazole (**B**) and diketopyrrolopyrrole (**D**), in an alternating arrangement to afford the donor-acceptor(1)-donor-acceptor(2) (**D-A-D-A′**) copolymer, **pTBTD**, as shown in **Scheme 1**. Diketopyrrolopyrrole and its isomer[7] have been reported as attractive acceptors in the development of semiconductors for use in high performance polymer-based organic field effect transistors (OFETs) and organic photovoltaics, exhibiting mobility and power conversion efficiency beyond 1 $cm^2 V^{-1} s^{-1}$[8–12] and 7%, respectively.[13–17] The **D-A-D-A'** nature of the new copolymers is expected to: i) lower the HOMO energy level of the polymer; ii) enhance intramolecular charge transfer, and iii) enhance π–π intermolecular interactions due to the coplanar nature of diketopyrrolopyrrole.[8,13,18]

Incorporation of branched side-chains improves polymer solubility compared with analogs with linear side chains.[1,2,19,20] However, branched side chains in which the branched point is close to the polymer backbone (e.g., 2-octyldodecyl, 2-decyltetradecyl) interferes with close packing of the polymers and weakens π–π intermolecular interactions between conjugated backbones, compared to analogs with linear side chains.[21–23] Therefore, a design strategy that

B. Fu, J. Baltazar, A. R. Sankar, P.-H. Chu, Prof. E. Reichmanis
School of Chemical & Biomolecular Engineering
Georgia Institute of Technology
311 Ferst Drive, Atlanta, GA 30332–0100, USA
E-mail: ereichmanis@chbe.gatech.edu
S. Zhang, Prof. D. M. Collard, Prof. E. Reichmanis
School of Chemistry & Biochemistry
Georgia Institute of Technology
901 Atlantic Drive, Atlanta, GA 30332–0400, USA
Prof. E. Reichmanis
School of Materials Science and Engineering
Georgia Institute of Technology
771 Ferst Drive, Atlanta, GA 30332–0245, USA

DOI: 10.1002/adfm.201304231

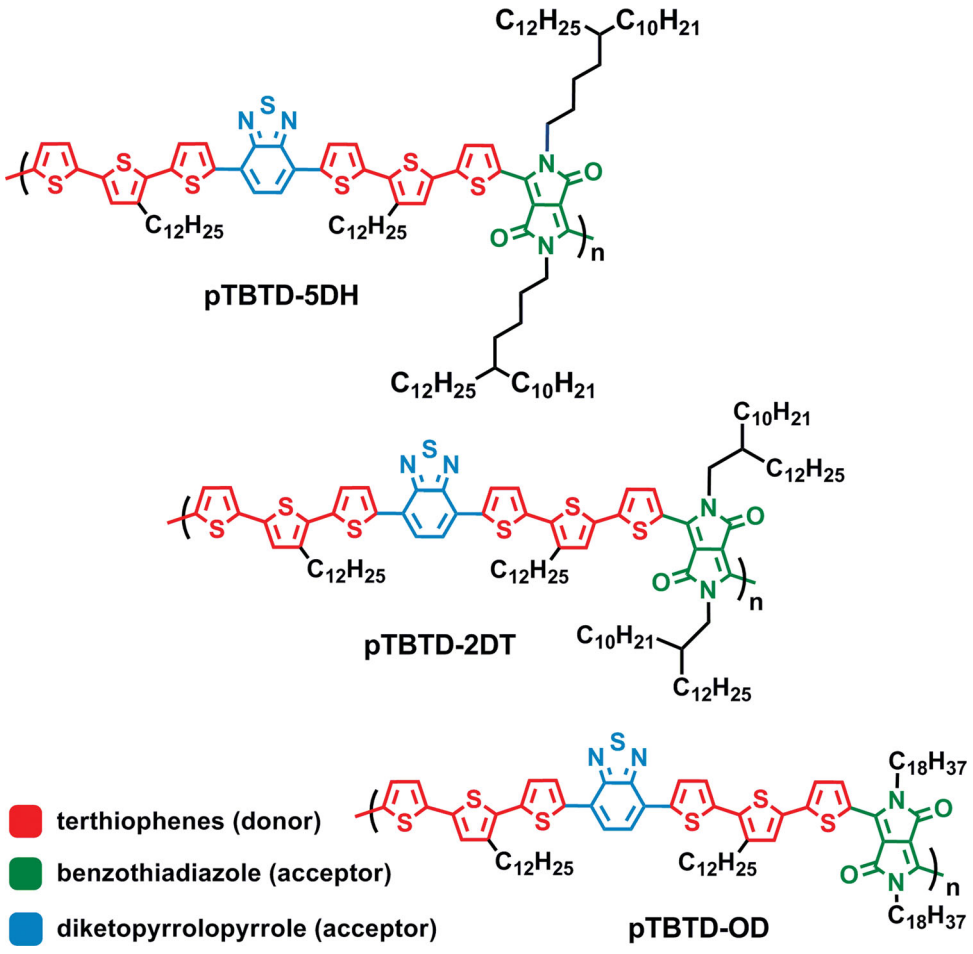

Scheme 1. Molecular structures of **TBTD** polymers substituted with branched side chains that are i) remote (**pTBTD-5DH**) or ii) close to (**pTBTD-2DT**) the conjugated polymeric backbone, and iii) the linear side chain (**pTBTD-OD**).

merges the advantages afforded by both linear and branched side chains is worthy of investigation. Here we describe the introduction of 5-decylheptadecyl (**5-DH**), 2-tetradecyl (**2-DT**), and *n*-octadecyl (**OD**) side chains onto the **TBTD** polymer, to afford **pTBTD-5DH**, **pTBTD-2DT**, and **pTBTD-OD**, respectively (Scheme 1). The side chain branching position is either remote (**5-DH**) or close (**2-DT**) to the polymer backbone. This design strategy of moving the branch point of the side chain away from the **pTBTD** backbone in **5-DH** was intended to reduce steric hindrance between chains while maintaining, or even improving, polymer solubility relative to that of analogous polymers with either branched (**2-DT**) or linear (**OD**) side chain. Recent reports have suggested the effectiveness of controlling the separation of branches in the side chain from the polymer backbone in tuning intermolecular self-assembly, charge carrier mobility,[24–26] and photocurrents.[27] A comparison of the properties of the three **pTBTD** analogs allows us to systematically investigate the effect of the variation of side chain structure on polymer solution processability, degree of polymerization, molecular ordering and orientation, and macroscopic charge carrier transport properties.

2. Results

2.1. Polymer Synthesis

The syntheses of the **TBTD** polymers are outlined in **Scheme 2**, and complete synthetic details are provided in the Supporting Information (S.I.). Commercially available 2-decyl-1-dodecanol, **1**, was converted to bromide **2**, which was then chain-extended by reaction with allylmagnesium chloride. The resulting alkene, **3**, was subjected to hydroboration–oxidation to afford alcohol **4**, which was subsequently converted to bromide **5**.[28] 3,6-Di(2-thienyl)diketopyrrolopyrrole, **6**, was alkylated with **5** to afford the **5-DH** substituted acceptor compound, **7a**, and with **2** and 1-bromooctadecane to afford **7b** and **7c**, respectively. It is noteworthy that the dialkylation of **6** with the 5-decyl-substituted compound to afford **7a** proceeds in high yield (>80%), which is similar to the yield of **7c** formed by alkylation of **6** with the linear side chain, and significantly higher than the yield of **7b** (30%) in which the side chain in the 2-position hinders nucleophilic substitution. The low yield for alkylation of diketopyrrolopyrrole with branched alkyl halides was recently reported as a common problem.[21,29,30]

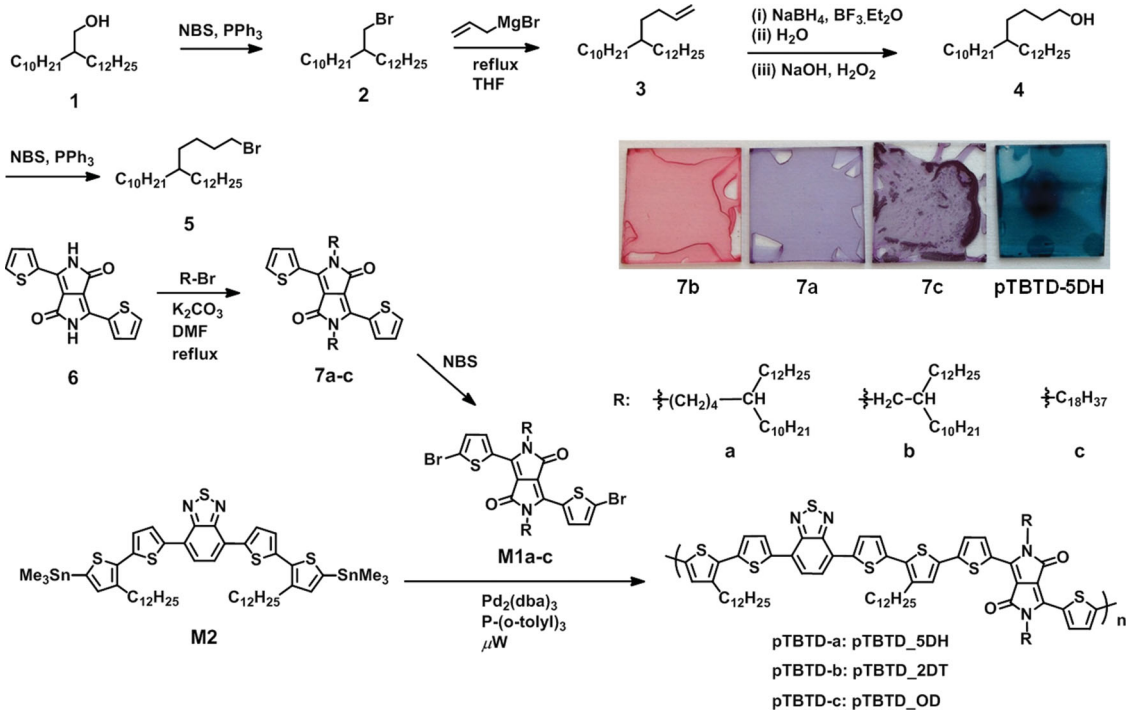

Scheme 2. Synthesis of **TBTD** polymers. Images inserted represent spin-coated films of compound **7a-c** (1500 rpm from 10 mg mL^{-1} in chloroform), and **pTBTD-5DH** (1500 rpm from 8 mg mL^{-1} in *o*-dichlorobenzene) on glass wafers.

Accordingly, moving the branching position further from the electrophilic site affords a more efficient monomer synthesis. Solutions of **7a-c** afforded similar absorption spectra (absorption maximum, λ_{max}, at 548 nm, Figure S1a, S.I.); while in the thin-film an obvious bathochromic shift was observed for the sequence of **7b** (pink, λ_{max} = 515 nm) to **7c** (purple, λ_{max} = 610 nm) and **7a** (purple, λ_{max} = 630 nm), as shown in Scheme 2 and Figure S1b, S.I. These results indicate that the steric hindrance arising from branching of the side chain close to the diketopyrrolopyrrole core (i.e., **2-DT**) disrupts π–π intermolecular interactions. Moving the branching away from diketopyrrolopyrrole unit (i.e., **5-DH**) relieves this hindrance and results in **7a** having a similar λ_{max} as the linear analog **7c**.

TBTD polymers were prepared by Stille step-growth polymerization of 3,6-di(5-bromo-2-thienyl)-*N*,*N*-dialkyldiketopyrrolopyrrole monomers **M1a-c** and bis-stannane monomer **M2**[6] under microwave irradiation (180 °C for 30 min, Scheme 2), followed by precipitation and subsequent purification by Soxhlet extraction. **pTBTD-5DH** was removed from the Soxhlet thimble with chloroform. The residue in the thimble was dissolved in hot 1,2-dichlorobenzene to afford a higher molecular weight sample, **pTBTD-5DH(H)**. The **2-DT** and **OD** analogs were prepared under the same conditions and extracted from the Soxhlet thimble with chloroform and chlorobenzene, respectively. Gel permeation chromatography (GPC; 135 °C with 1,2,4-trichlorobenzene as eluent, **Table 1**) gave number-average molecular weights (M_n) of **pTBTD-5DH** and **pTBTD-5DH(H)** of 44 kg mol^{-1} and 50 kg mol^{-1}, respectively, approximately twice that of **pTBTD-2DT** (28 kg mol^{-1}) and four times that of **pTBTD-OD** (14 kg mol^{-1}) prepared in the same manner. This result suggests that the **5-HD** side chains allow the polymerization to proceed to give higher molecular weight by maintaining solubility of the growing polymer. No shoulders were observed on the GPC peaks (Figure S2 in S.I.), indicative of no aggregation of polymer chains. Efforts to prepare lower molecular weight **pTBTD-5DH** using milder reaction conditions (160 °C for 30 min), afforded samples exhibiting no substantial change in M_n (44 kg mol^{-1}, PDI: 2.3, Figure S2e, S.I.), suggesting that the incorporation of **5-DH** facilitates preparation of relatively high molecular weight polymers, a desirable characteristic for high performance polymer semiconductors.[31,32]

Table 1. Molecular weights and photophysical properties of **TBTD** polymers.

Polymer	M_n [kDa]	PDI	DP[a)]	Absorption maximum [eV]		E_g^{opt} [eV][b)]
				Solution	Film	
pTBTD-5DH	44	2.3	24	1.60, 2.99	1.58, 1.72, 2.98	1.26
pTBTD-5DH(H)	50	2.1	27	1.60, 2.99	1.58, 1.72, 2.98	1.26
pTBTD-2DT	28	2.5	16	1.60, 1.72, 3.03	1.58, 1.73, 2.97	1.30
pTBTD-OD	14	2.5	9	1.94, 3.24	1.56, 1.69, 2.93	1.26

[a)]Degree of polymerization, calculated from M_n divided by molecular weight of repeating unit; [b)]optical bandgap, estimated from the thin film absorption band onset point (λ_{onset}): $E_{opt} = 1240/\lambda_{onset}$.

2.2. Photophysical Properties

The UV-visible absorption spectra of the **TBTD** polymers are shown in **Figure 1**. In

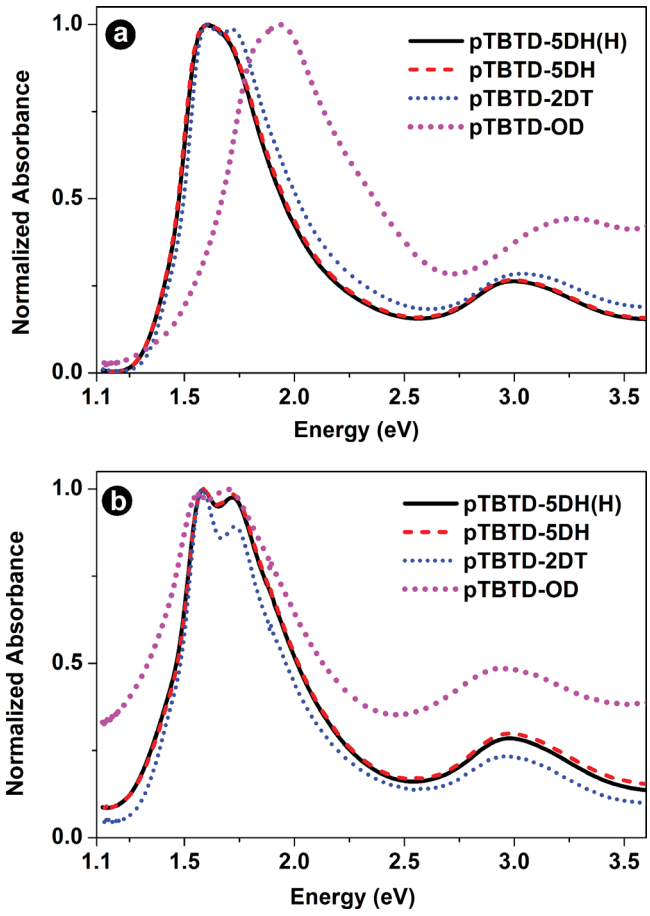

Figure 1. Absorption spectra of **TBTD** polymers: a) in solution (1,2-dichlorobenzene) at room temperature; and b) thin film at room temperature.

solution (Figure 1a), **pTBTD-5DH** exhibits a similar absorption onset as **pTBTD-2DT**, suggesting a similar extent of π-conjugation within the polymer backbone. The absorption maximum analog with linear side chains, **pTBTD-OD**, is shifted to higher energy by 0.33 eV in comparison to the maxima of **pTBTD-5DH** and **pTBTD-2DT**. For thin films (Figure 1b), the absorption maximum of **pTBTD-OD** is red-shifted by 0.23 eV compared to the maximum recorded in solution, consistent with planarization of the polymer backbone and enhanced π–π interchain interactions. Both **pTBTD-5DH** and **pTBTD-OD** exhibit relatively lower optical bandgaps (E_g^{opt}, 1.26 eV in Table 1) than **pTBTD-2DT** (1.30 eV) in thin-film form. This suggests that moving the branching of side chains away from the polymer backbone enhances π-conjugation compared to analogs in which the branching is close to the conjugated backbone; and provides **pTBTD-5DH** with photophysical properties that are similar to the analog with linear side chains. Finally, it should be noted that the absorption peaks of films of **pTBTD-OD** exhibit a significant tail due to reflectivity. This arises from the low solubility of the linear side chain polymer analog, which results in formation of films with high surface roughness. All of the **pTBTD** polymers were thermally annealed at between 100 and 300 °C under inert atmosphere (Figure S3, S.I.); no change was observed in the absorption spectra upon annealing, demonstrating the high thermal stability of the films.

2.3. Electrochemistry

Cyclic voltammetry (CV) and differential pulse voltammetry (DPV) were employed to investigate the redox properties of thin films of **TBTD** polymers (Figure S4, S.I.). All of the **pTBTD** polymers exhibited an oxidation onset between 0.41 and 0.54 V versus Fc/Fc^+ (–4.8 eV versus vacuum) by CV, and between 0.45 and 0.50 V versus Fc/Fc^+ by DPV, as shown in **Table 2**. These values correspond to HOMO energy levels of –5.2 to –5.3 eV. The oxidation of all of the **pTBTD** polymers displayed good reversibility (e.g., **pTBTD-5DH** shown in **Figure 2**), demonstrating the oxidative stability of these polymers. **pTBTD-5DH** (Figure 2 and Figure S4, S.I.) and **pTBTD-OD** (Figure S4, S.I.) exhibited a second oxidation peak at between 1.2 and 1.4 eV versus Fc/Fc^+, suggesting the presence of both polaronic and bipolaronic states in these polymers. No reduction peaks were evident in the CV or DPV of these materials.

2.4. Ionization Potentials

The HOMO energy levels determined by CV and DPV include the impact of penetration of the electrolyte which swells the polymer films, and thereby changing film morphology during the oxidation process.[33,34] Accordingly, we chose to characterize films of **pTBTD** polymers by ultraviolet photoelectron spectroscopy (UPS) to determine the intrinsic work functions (ϕ) and ionization potentials (IP) (Figure S5, S.I.). The resulting HOMO energy levels of **pTBTD** are between at –4.9 and –5.1 eV for as-spun films (Table 2), which are approximately

Table 2. Redox properties, HOMO, LUMO, and work-function energy levels of *TBTD* polymers.

Polymers	CV			DPV			UPS				LUMO[e] [eV]
	$1^{st}E_{ox}$[a] [V]	$2^{nd}E_{ox}$[b] [V]	HOMO [eV]	$1^{st}E_{ox}$[c] [V]	$2^{nd}E_{ox}$[d] [V]	HOMO [eV]	$IP_{as\text{-}spun}$ [eV]	$\phi_{as\text{-}spun}$ [eV]	$IP_{annealed}$ [eV]	$\phi_{annealed}$ [eV]	
pTBTD-5DH	0.47	1.23	–5.27	0.45	1.35	–5.25	5.04	4.46	4.94	4.31	3.78
pTBTD-2DT	0.54	n/a	–5.34	0.49	n/a	–5.29	5.04	4.52	4.86	4.28	3.74
pTBTD-OD	0.41	n/a	–5.21	0.5	1.38	–5.3	5.06	4.59	4.95	4.32	3.8

[a] 1st oxidation peak upon CV; [b] 2nd oxidation peak upon CV; [c] 1st oxidation peak upon DPV; [d] 2nd oxidation peak upon DPV; [e] LUMOs were calculated from $IP_{as\text{-}spun}$ substituted by E_g^{opt} (Table 1).

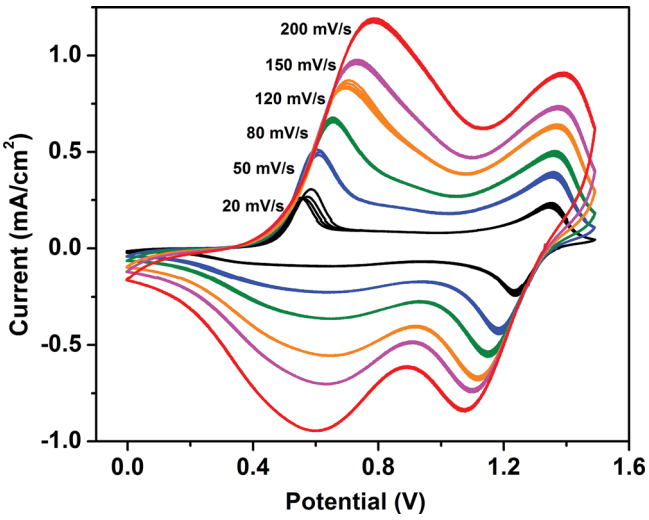

Figure 2. Cyclic voltammograms of a drop-cast film of **pTBTD-5DH** on a platinum electrode (in 0.5M Bu_4NPF_6/acetonitrile) at scan rates between 20 mV s^{-1} and 200 mV s^{-1} (five cycles at each scan rate).

0.2–0.3 eV higher than those obtained by CV and DPV. After thermal annealing, **pTBTD-5DH**, **pTBTD-2DT**, and **pTBTD-OD** exhibited a ≈ 0.1 eV decrease in IP to between 4.8 and 5.0 eV. This decrease is attributed to enhancement of molecular ordering upon thermal annealing, confirmed by subsequent X-ray scattering and AFM characterization (vide infra). LUMO energy levels of **pTBTD** are ≈ –3.7 eV, based upon the common estimation that $E_{LUMO} = E_{HOMO} - E_g^{opt}$ (optical bandgap), without consideration of the exciton binding energy (0.3–1.0 eV).[35,36]

2.5. Thermal Properties

The **TBTD** polymers decompose at temperatures greater than 360 °C (see TGA characterization, **Table 3** and Figure S6a, S.I.), indicative of high thermal stability. All **TBTD** polymers show the presence of two endothermic transitions upon heating (T_{h1} and T_{h2}), and two exothermic transitions during the cooling process (T_{c1} and T_{c2}, see DSC characterization, Table 3 and Figure S6b–d, S.I.), revealing the presence of ordered phases. The lower temperature transitions (T_{h1} and T_{c1}) most likely correspond to the disordering and reordering processes associated with the side chains; while those at higher temperature (T_{h2} and T_{c2}) represent a polymer backbone phase transition before entering an isotropic phase. X-ray scattering (vide infra) indicated an improvement in crystallinity and molecular ordering of **TBTD** polymers after thermal annealing beyond T_{h2} and T_{c2} and at up to 350 °C, suggesting that the melting point of the **TBTD** polymers is even higher (above the onset of decomposition).

2.6. Thin-Film Crystallinity and Morphology

Polymer thin-film microstructures were investigated by two-dimensional grazing incidence wide angle X-ray scattering (2D-GIWAXS, **Figure 3**). Films were prepared by drop-casting 1,2-dichlorobenzene-solutions of the polymers onto a Si substrate (300 nm SiO_2 dielectric on heavily p-doped Si) that had been pre-functionalized with octadecyltrichlorosilane (OTS-18). All **TBTD** polymers exhibited well-defined (*h*00) diffraction patterns along the q_z (out-of-plane) axis corresponding to a highly ordered lamellar structure; and (010) peaks along the q_{xy} (in-plane) axis arising from *π*–*π* stacking of polymer backbones. For example, **pTBTD-5DH(H)**, exhibits a (100) peak at $2\theta = 3.59°$, (200) at $2\theta = 7.17°$, (300) at $2\theta = 10.75°$, and (400) at $2\theta = 14.37°$, corresponding to a lamellar *d*-spacing distance of 24.55 Å between polymer chains segregated by a combination of **5-DH** and dodecyl side chains (on the diketopyrrolopyrrole units and thiophene units, respectively). A (010) peak at $2\theta = 24.79°$ indicates a 3.59 Å *π*–*π* stacking distance. Results for other **TBTD** polymers are shown in **Table 4**. The lamellar spacing suggests that the polymer side-chains are highly interdigitated in the crystalline phase. Similar to our benchmark polymer, **pBT6**,[6] the variation of intensity of **pTBTD** at $2\theta \approx 24.5°$ along the γ axis indicates high (010) peak intensity in the in-plane direction, and a very low intensity in the out-of-plane direction (Figure S7, S.I.). These results suggest the formation of highly ordered lamellar structures with edge-on orientation relative to the substrate surface (Scheme S1, S.I.). **pTBTD-5DH** and **pTBTD-5DH(H)**, in which the branching of side chain is remote from the backbone exhibit a similar *π*–*π* stacking distance (3.6 Å) to the linear analog, **pTBTD-OD** (3.62 Å), which is smaller than the **2-DT** analog (3.73 Å). These results reveal a benefit derived from moving the branching position further from the polymer backbone whereby steric hindrance that impedes *π*–*π* stacking in the **2-DT**-substituted polymer is relieved in the **5-DH** analog, thereby allowing for closer *π*–*π* intermolecular interactions between conjugated chains. This is a critical feature for enhancing charge carrier transport. Thermal annealing of the **TBTD** polymers resulted in an increase in the intensity of both the (*h*00) and (010) diffraction peaks, signifying an increase in the degree of crystallinity. The full-width-at-half-maximum (FWHM) of the (100) diffraction peak (Table 4) decreased upon thermal annealing,

Table 3. Thermal decomposition temperature (T_d) and thermal transition temperatures (T_g[a)], T_h[b)], and T_c[c)]) of **TBTD** polymers.

Polymer	T_d/°C	T_g/°C	Heating		Cooling	
			T_{h1} [°C] (ΔH, J g^{-1})	T_{h2} [°C] (ΔH, J g^{-1})	T_{c1} [°C] (ΔH, J g^{-1})	T_{c2} [°C] (ΔH, J g^{-1})
pTBTD-5DH	412	n/a	–44 (3.76)	70	–47 (1.31)	65
pTBTD-2DT	400	32	–4 (0.1)	91 (0.3)	–38 (0.2)	61 (0.3)
pTBTD-OD	360	n/a	–6 (3.3)	90 (0.1)	–11 (4.9)	62 (0.1)

[a)] T_g: glass transition temperature; [b)] T_h: phase transition temperature upon heating process; [c)] T_c: phase transition temperature upon cooling process.

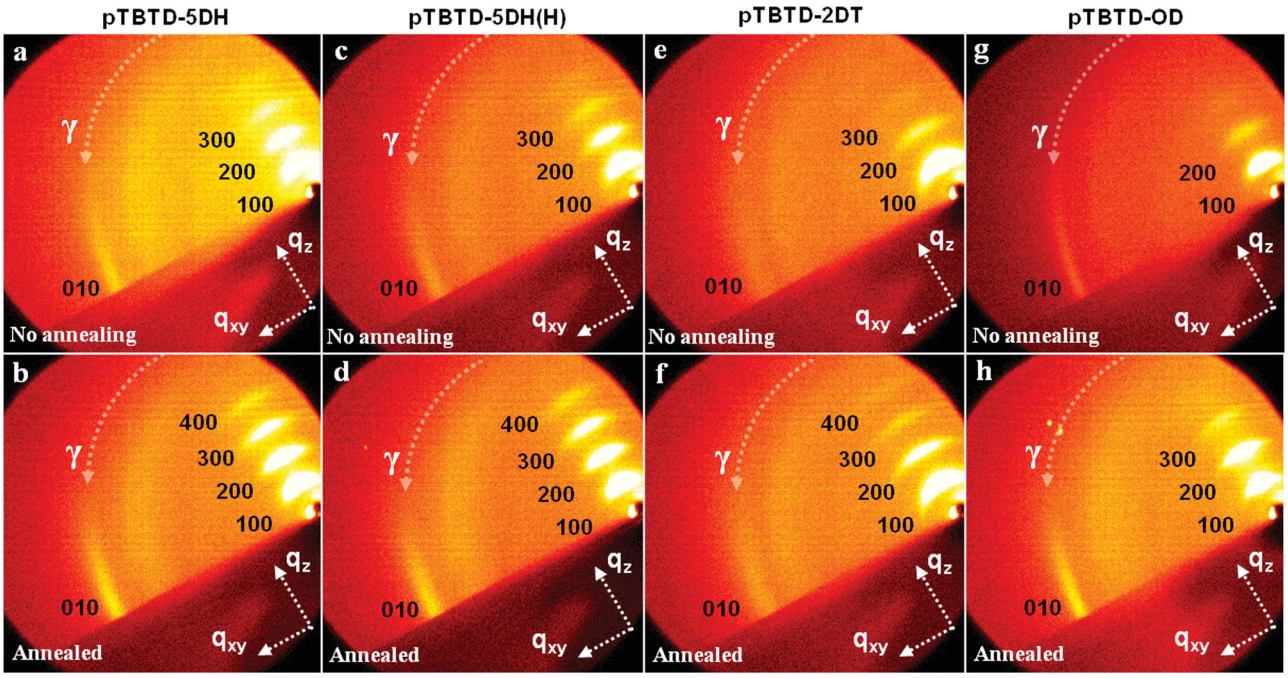

Figure 3. 2D-GIWAXS area detector images of **pTBTD** drop-cast films: a,b) **pTBTD-5DH**; c,d) **pTBTD-5DH(H)**; e,f) **pTBTD-2DT**; g,h) **pTBTD-OD**. Top row, as-spun films; bottom row, samples after annealed at 200 °C (**pTBTD-OD** at 300 °C) for 30 min followed by rapidly cooled to room temperature.

Table 4. 2D-GIWAXS peak assignments and corresponding distances of **TBTD** polymers before and after thermal annealing.

Polymer	As-spun film				After annealing[a)]			
	2θ [°]		distance [nm]	FWHM	2θ [°]		distance [nm]	FWHM
pTBTD-5DH(H)	3.55	(100)	24.88	0.73	3.60	(100)	24.55	0.45
	7.13	(200)			7.17	(200)		
	10.66	(300)			10.7	(300)		
	n/a				14.3	(400)		
	24.75	(010)	3.59		24.79	(010)	3.59	
pTBTD-5DH	3.55	(100)	24.88	0.66	3.55	(100)	24.88	0.48
	7.04	(200)			7.09	(200)		
	10.58	(300)			10.61	(300)		
	n/a				14.11	(400)		
	24.55	(010)	3.62		24.66	(010)	3.61	
pTBTD-2DT	4.10	(100)	21.56	0.95	4.00	(100)	22.07	0.64
	8.22	(200)			7.95	(200)		
	12.21	(300)			11.94	(300)		
	n/a				15.83	(400)		
	24.18	(010)	3.68		23.84	(010)	3.73	
pTBTD-OD	3.96	(100)	22.29	0.97	3.96	(100)	22.29	0.43
	7.90	(200)			7.99	(200)		
	n/a				12.01	(300)		
	24.76	(010)	3.59		24.60	(010)	3.62	

[a)] **pTBTD-5DH** and **pTBTD-2DT** were annealed at 200 °C for 30 min; **pTBTD-5DH(H)** and **pTBTD-OD** were annealed at 300 °C for 30 min.

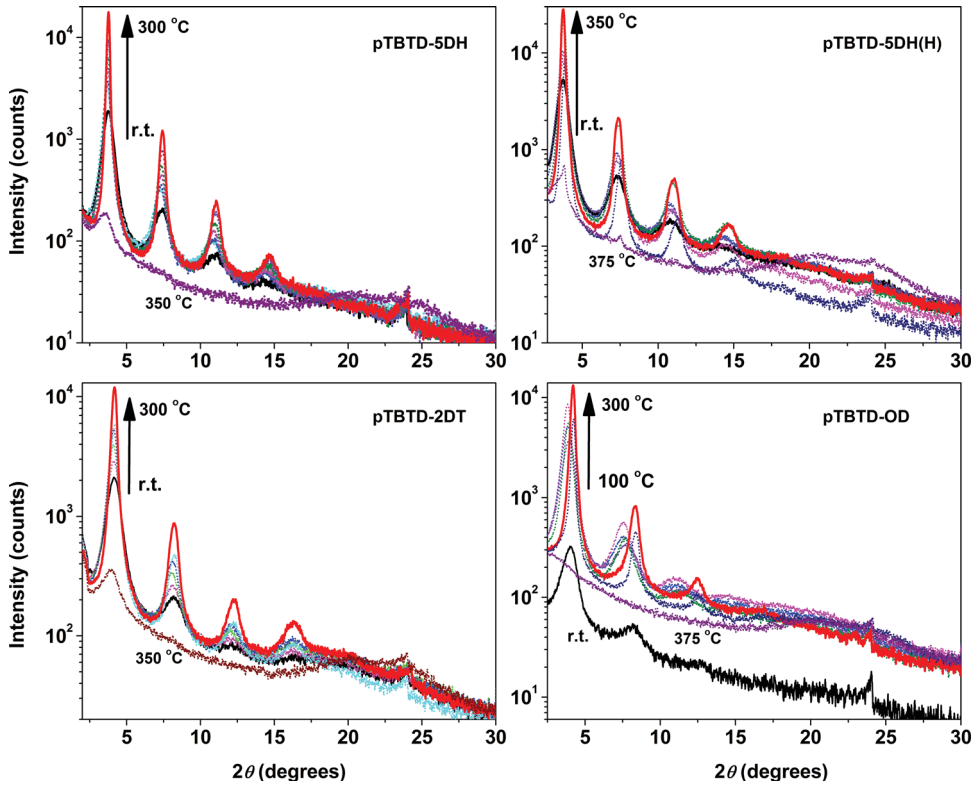

Figure 4. 1D-GIXS patterns of **pTBTD** drop-cast films. Films were drop-casted at room temperature; annealed at 100 °C for 30 min, then at 150 °C, 200 °C, 250 °C, 300 °C, 350 °C, and 375 °C for 30 min at each temperature.

corresponding to an increase of the coherence length of crystalline domains along the (100) axis.[37,38]

To gain further understanding of the impact of thermal annealing on the molecular ordering of **TBTD** polymers, films were annealed at 100–375 °C and characterized using one-dimensional grazing incidence X-ray scattering (1D-GIXS), as shown in **Figure 4**. Upon increasing the annealing temperature to as high as 375 °C, a temperature close to the onset of decomposition (vide supra), all of the **TBTD** polymers exhibited an increase in the intensity of the (*h*00) lamellar diffraction peak with a concomitant decrease in the FWHM of the (*h*00) diffraction peaks (**Figure 5**a).

The surface morphologies of **TBTD** polymer films were explored using tapping-mode atomic force microscopy (AFM), as shown in **Figure 6** (phase images) and Figure S8b (S.I., height images). Polymer films were spin-coated onto Si substrates (300 nm SiO_2 dielectric on heavily p-doped Si) that had been pre-functionalized with OTS-18. The as-spun films appeared highly ordered with a nano-fibrillar texture for **pTBTD-5DH**, **pTBTD-5DH(H)**, and **pTBTD-2DT**, and a

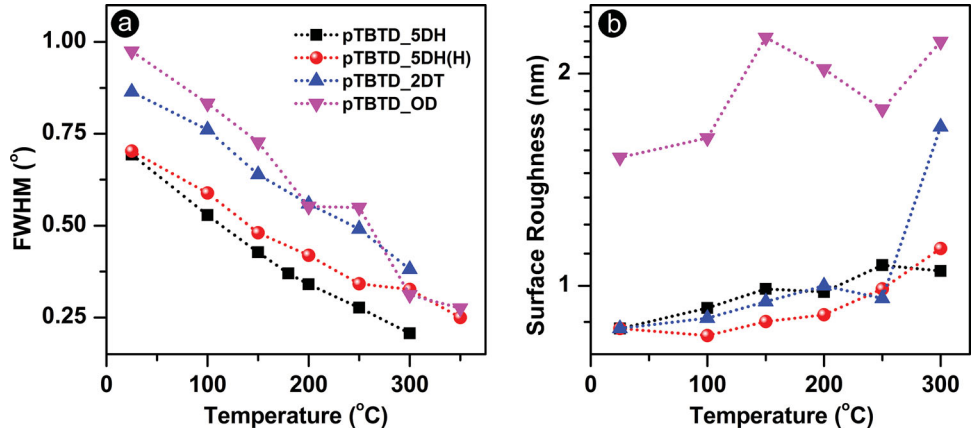

Figure 5. a) FWHM of (100) diffraction peak of **TBTD** polymer films via 1 D-GI XS as a function of annealing temperature; b) surface roughness of **TBTD** polymer films measured by tapping mode AFM as a function of annealing temperature.

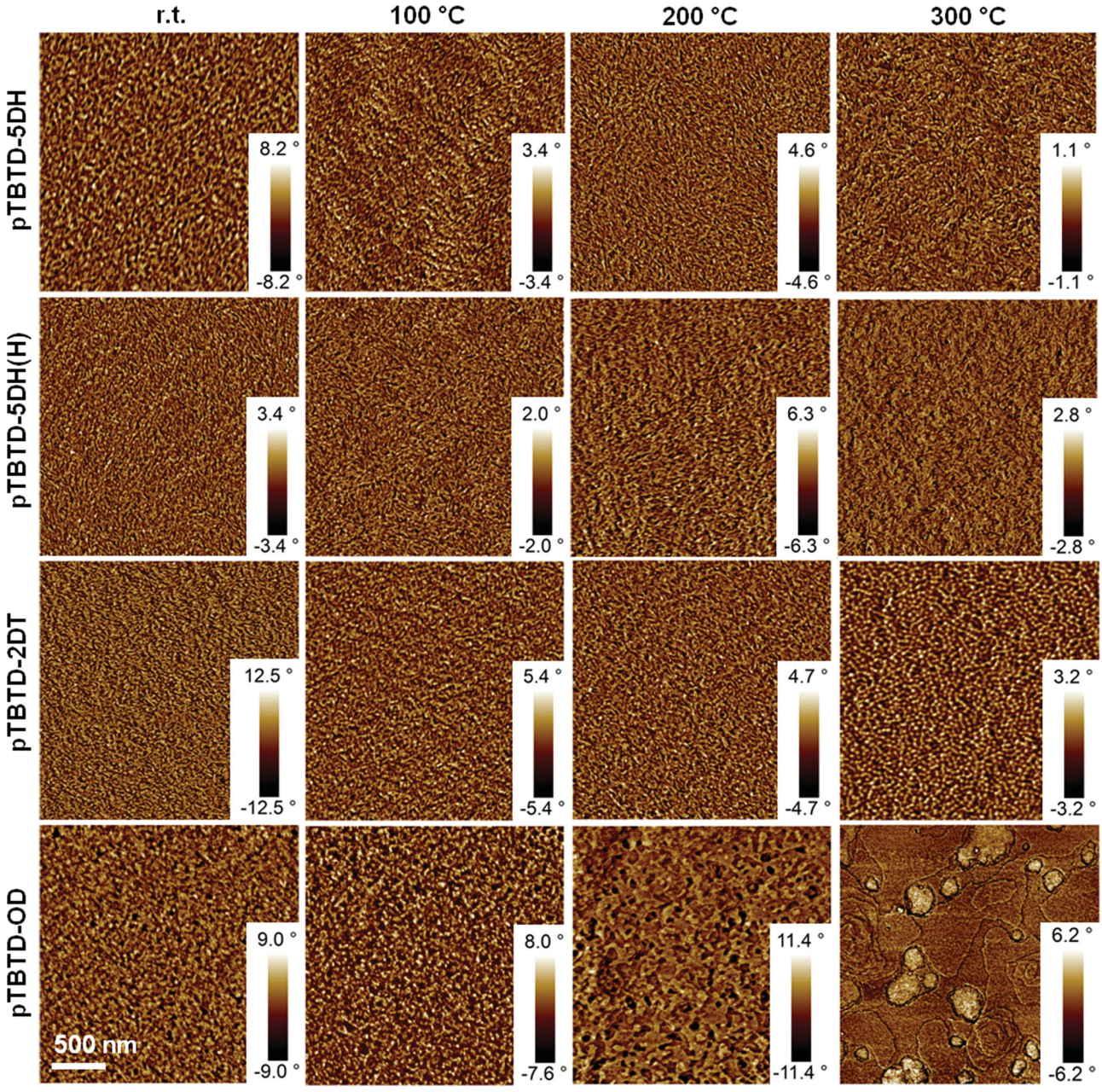

Figure 6. Tapping mode AFM phase images of **TBTD** polymers recorded as as-spun films (r.t.) and after annealing at 100 °C, 200 °C, and 300 °C for 30 min at each temperature followed by rapidly cooled to room temperature. Results recorded at room temperature after annealing at 150 °C and 250 °C for 30 min at each temperature are shown in Figure S8a, S.I.

nano-granular character was observed for the linear side chain analog, **pTBTD-OD**, which are consistent with the high crystallinity revealed by GIXS. All polymer films prepared here exhibited an increase in surface roughness with increased annealing temperature over the range of 100 to 300 °C (Figure 5b), further supporting an increase in crystallinity and molecular ordering. In combination, the results from GIXS and AFM indicate that the degree of crystallinity and grain size of **TBTD** polymer can be improved by annealing at temperatures up to 300–350 °C. Given the importance of molecular order in determining the charge transport in π-conjugated polymers, we went on to investigate the impact of thermal annealing on the charge carrier transport properties.

2.7. Field-Effect Mobility

The charge carrier transport properties of the **TBTD** polymers were investigated using a bottom-contact-bottom-gate organic field-effect transistor (OFET) device architecture. Solutions of the polymers in 1,2-dichlorobenzene (5–8 mg mL^{-1}) were spin-coated or drop-cast onto OFET substrates (300 nm

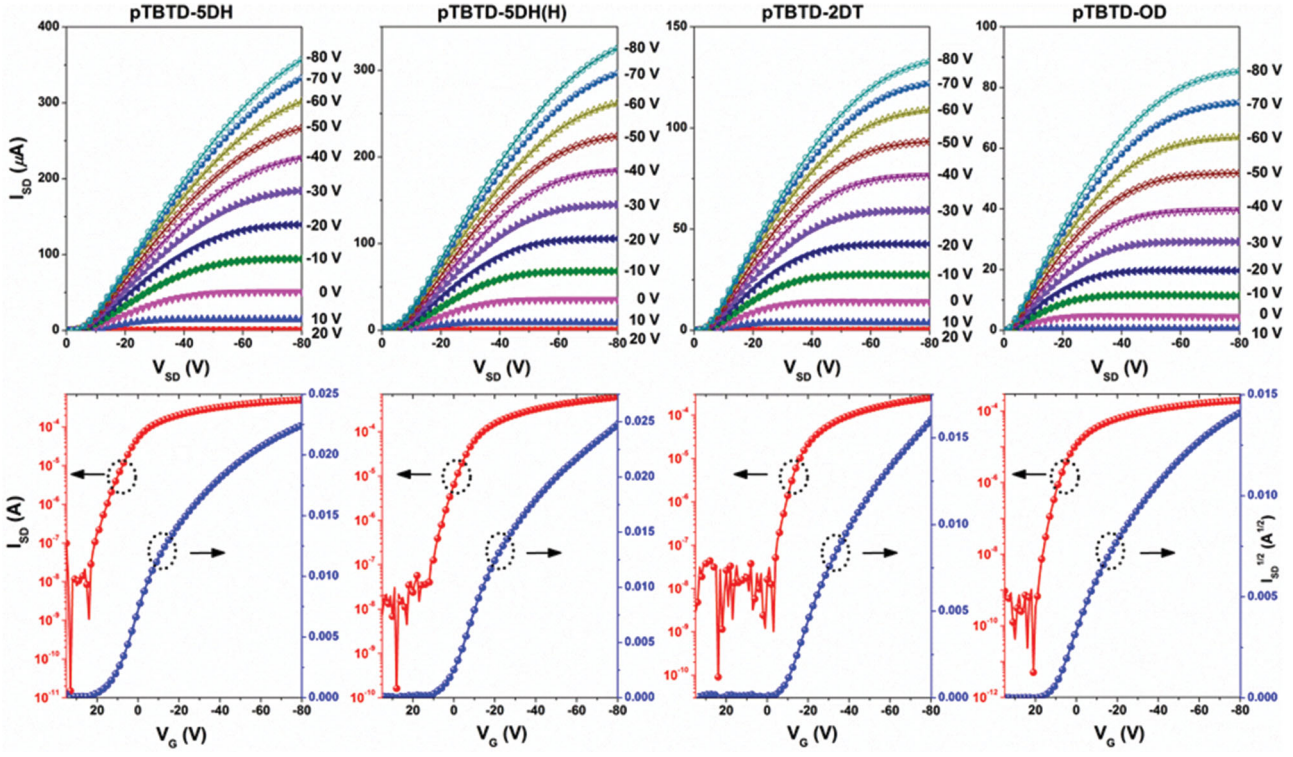

Figure 7. Output (top row) and transfer (bottom row, $V_{SD} = -80$ V) **TBTP** polymers measured in OFETs with channel size of 50 μm long × 2 mm wide.

of SiO_2 dielectric grown on heavily n-doped Si) that had been pre-treated with OTS-18 (see fabrication details in S.I.). The channel between gold source and drain electrodes was 50 μm long and 2 mm wide. **pTBTD-5DH** and **pTBTD-5DH(H)** are more soluble in 1,2-dichlorobenzene than **pTBTD-2DT** and **pTBTD-OD**, indicating that the **5-DH** side chain maintains solubility of the polymer that is observed for other branched chains. **pTBTD-OD** did not fully dissolve even upon heating solution to 145 °C, leading to formation of non-uniform films. The output and transfer curves for devices fabricated with the **TBTD** polymers are shown in **Figure 7**, and the resulting mobilities calculated from the saturation regime are listed in **Table 5** (and Table S1 in S.I.). **pTBTD-5DH** and **pTBTD-5DH(H)** exhibited higher field effect hole mobilities than **pTBTD-2DT** and **pTBTD-OD**. In particular, **pTBTD-5DH(H)** exhibited average and maximum hole mobility measurements of 2.32 and 2.95 $cm^2\ V^{-1}\ s^{-1}$ after annealing devices at 300 °C for 30 min. These values are ≈ 3–4× greater than those recorded for **pTBTD-2DT** (average, 0.4 $cm^2\ V^{-1}\ s^{-1}$; maximum, 0.81 $cm^2\ V^{-1}\ s^{-1}$) and ≈ 8× the mobility of **pTBTD-OD** (average, 0.3 $cm^2\ V^{-1}\ s^{-1}$, maximum, 0.34 $cm^2\ V^{-1}\ s^{-1}$). The significant increase in mobility has its origin in the combination of improved polymer solubility, enhanced π–π intermolecular interactions, and an increased degree of polymerization that result from the presence of branching of the side chain remote from the conjugated main chain of the polymer.

Table 5. Hole-transport properties of **TBTD** polymers based OFET devices.[a)]

Samples	Annealing temp[b)] [°C]	Film processing	Hole mobility [$cm^2\ V^{-1}\ s^{-1}$]		$I_{ON/OFF}$	$V_{TH,\ avg}$ [V]
			Avg	Max		
pTBTD-5DH(H)	n/a	spin-coat	1.02	1.34	10^4–10^6	11.7
	300	spin-coat	2.32	2.95	10^5–10^6	12.8
pTBTD-5DH	n/a	spin-coat	0.62	0.68	10^5–10^7	–13.2
		drop-cast	0.43	0.62	10^5–10^6	–0.5
	300	spin-coat	1.74	2.00	10^5–10^6	13.1
		drop-cast	1.06	1.21	10^5–10^7	5.4
pTBTD-2DT	n/a	spin-coat	0.49	0.77	10^6–10^6	8.8
		drop-cast	0.32	0.48	10^5–10^7	–21.4
	300	spin-coat	0.40	0.54	10^6–10^7	–2.7
		drop-cast	0.40	0.81	10^5–10^7	–7
pTBTD-OD	n/a	spin-coat	0.05	0.07	10^4–10^5	7.3
		drop-cast	0.04	0.06	10^3–10^5	6.4
	300	spin-coat	0.30	0.34	10^6–10^7	7
		drop-cast	0.16	0.27	10^4–10^6	–4.6

[a)]Characterization results were based on 5–8 of devices for each fabrication conduction; [b)]OFET devices were thermally annealed at 300 °C for 30 min. "n/a" denotes no annealing (as-spun films). The results of thermal annealing at 100–250 °C are listed in Table S1 (see S.I.).

OFET devices fabricated with the series of **TBTD** polymers were annealed at temperatures ranging from 100 to 300 °C to further understand the impact of thermally induced molecular ordering on charge carrier transport (Table S1, S.I.) **pTBTD-5DH(H)**, **pTBTD-5DH**, and **pTBTD-OD** exhibited an increase in hole mobility upon increasing the annealing temperature (Figure S9, S.I.) For example, **pTBTD-5DH(H)** exhibited a hole mobility of up to 2.95 $cm^2 V^{-1} s^{-1}$ after annealing at 300 °C compared to an average mobility of 1.02 $cm^2 V^{-1} s^{-1}$ for as-spun films. However, no mobility improvement was observed upon thermal treatment of **pTBTD-2DT** .

Drop cast films showed a ≈30–40% lower hole mobility than spin coated films (Table 5 and Table S1), a trend which is opposite to that observed for the parent **pBT6**.[6] This may be explained by the formation of polycrystalline thick films of the **pTBTD** polymers during the slow solvent evaporation associated with drop casting (see experimental details in S.I.). Grain boundaries in such films block efficient charge carrier hopping and result in lower mobilities.[39,40]

3. Discussion

The characterization results of **TBTD** polymers raises important points regarding side chain engineering as an approach to optimize the semiconducting properties of conjugated polymers. First, incorporation of an alkyl branch remote from the conjugated polymer backbone, illustrated here with the **5-DH** side chain, provides materials (i.e., **pTBTD-5DH**) with a solubility that is close (or even superior) to that of polymers bearing side chains that are branched close to the backbone (e.g., **2-DT** side chains on **pTBTD-2DT**). The solubility of the **TBTD** polymer series follows the sequence of **pTBTD-5DH** (and **pTBTD-5DH(H)**) ≥ **pTBTD-2DT** >> **pTBTD-OD**. This solubility improvement has two notable consequences: (i) the polymerization of **pTBTD-5DH** proceeds to higher molecular weight, and (ii) **pTBTD-5DH** gives rise to higher quality films than **pTBTD-OD**.

Second, **5-DH** side-chains impart **pTBTD-5DH** (and its corresponding dithienyldiketopyrrolopyrrole derivative **7a**) with π–π intermolecular interactions similar to that of the linear 1-octadecyl analog, **pTBTD-OD** (and its corresponding dithienyldiketopyrrolopyrrole derivative **7c**). This is in contrast to the case of the side chain with a branch position proximal to the backbone, **pTBTD-2DT** (and **7b**), as has also been reported for a different D-A conjugated polymer by Fréchet et al.[19] The interchain distances follow the sequence of **pTBTD-5DH** (3.6 Å) ≈**pTBTD-OD** (3.62 Å) < **pTBTD-2DT** (3.73 Å) from 2D-GIWAXS; and compounds **7a** and **7c** are bathochromatically shifted from **7b** (Scheme 2 and Figure S1b, S.I.) in the film state.

Thus, the use of side chains in which branch points are incorporated remote from the polymer backbone combines the superiority of branched side chains to improve polymer solubility (and in turn the degree of polymerization) with that of linear chains in facilitating dense π–π interchain stacking by lowering steric hindrance. In contrast, side chains that are branched close to the backbone increase steric hindrance, and linear side-chains limit solubility. Efficient charge carrier transport within polymeric semiconductors requires strong microscale π–π intermolecular interactions for effective charge carrier hopping; and good polymer solubility to facilitate formation of dense, continuous films and thereby avoid macroscale thin-film structural defects.[41] The side chains of **pTBTD-5DH** provide this combination of features to afford a material with significantly higher charge carrier mobility than **pTBTD-2DT** and **pTBTD-OD** in OFET devices.

4. Conclusion

We have developed a low bandgap **D-A-D-A′** polymer semiconductor, **pTBTD**, in which a linear side chain (**OD**) and side chains with branches remote (**5-DH**) and proximal (**2-DT**) were incorporated onto the backbone to afford **pTBTD-5DH**, **pTBTD-2DT**, and **pTBTD-OD**, respectively. The systematic investigation of these three polymers demonstrates, for the first time, that the incorporation of side chains in which the branch position is remote from the polymer backbone combines the benefit of branched side chains in improving solubility with linear chains in promoting efficient π–π inter-molecular interactions. This provides a polymer with enhanced solution processability, a higher degree of polymerization, close π–π intermolecular stacking, and, in turn, superior macroscale charge carrier transport. These results underscore the significance of understanding structure-property relationships associated with the structure of side chains on conjugated polymers, and demonstrate the promising potential of developing high-performance organic semiconductors via side chain engineering.

Supporting Information

Supporting Information is available from the Wiley Online Library or from the author.

Acknowledgement

The authors gratefully acknowledge the contributions of Professor Richard Jordan and Ge Feng of the Department of Chemistry at the University of Chicago (high temperature GPC characterization); and Professor John R. Reynolds and Kin Lo of the School of Chemistry and Biochemistry at the Georgia Institute of Technology (CV and DPV characterization). This research was funded in part by the Georgia Institute of Technology, the Center for Organic Photonics and Electronics (COPE) at Georgia Tech, and the National Science Foundation (DMR-1207284). 2D-GIXS measurements were carried out by Linda Sauer at the Characterization Facility, University of Minnesota, which receives partial support from NSF through the MRSEC program.

Received: December 19, 2013
Revised: January 27, 2014
Published online: March 19, 2014

[1] P. M. Beaujuge, J. M. J. Frechet, *J. Am. Chem. Soc.* **2011**, *133*, 20009.
[2] J. Mei, Z. Bao, *Chem. Mater.* **2014**, *26*, 604.
[3] J. G. Mei, Y. Diao, A. L. Appleton, L. Fang, Z. N. Bao, *J. Am. Chem. Soc.* **2013**, *135*, 6724.
[4] T. Lei, J. H. Dou, J. Pei, *Adv. Mater.* **2012**, *24*, 6457.

[5] J. G. Mei, D. H. Kim, A. L. Ayzner, M. F. Toney, Z. A. Bao, *J. Am. Chem. Soc.* **2011**, *133*, 20130.
[6] B. Y. Fu, J. Baltazar, Z. K. Hu, A. T. Chien, S. Kumar, C. L. Henderson, D. M. Collard, E. Reichmanis, *Chem. Mater.* **2012**, *24*, 4123.
[7] S. Lu, M. Drees, Y. Yao, D. Boudinet, H. Yan, H. Pan, J. Wang, Y. Li, H. Usta, A. Facchetti, *Macromolecules* **2013**, *46*, 3895.
[8] C. B. Nielsen, M. Turbiez, I. McCulloch, *Adv. Mater.* **2013**, *25*, 1859.
[9] X. Guo, S. R. Puniredd, M. Baumgarten, W. Pisula, K. Mullen, *Adv. Mater.* **2013**, *25*, 5467.
[10] J. Li, Y. Zhao, H. S. Tan, Y. L. Guo, C. A. Di, G. Yu, Y. Q. Liu, M. Lin, S. H. Lim, Y. H. Zhou, H. B. Su, B. S. Ong, *Sci. Rep.* **2012**, *2*, 754.
[11] J. D. Yuen, J. Fan, J. Seifter, B. Lim, R. Hufschmid, A. J. Heeger, F. Wudl, *J. Am. Chem. Soc.* **2011**, *133*, 20799.
[12] J. H. Kim, D. H. Lee, D. S. Yang, D. U. Heo, K. H. Kim, J. Shin, H.-J. Kim, K.-Y. Baek, K. Lee, H. Baik, M. J. Cho, D. H. Choi, *Adv. Mater.* **2013**, *25*, 4102.
[13] Y. N. Li, P. Sonar, L. Murphy, W. Hong, *Energy Environ. Sci.* **2013**, *6*, 1684.
[14] A. Facchetti, *Chem. Mater.* **2011**, *23*, 733.
[15] L. T. Dou, J. B. You, J. Yang, C. C. Chen, Y. J. He, S. Murase, T. Moriarty, K. Emery, G. Li, Y. Yang, *Nat. Photonics* **2012**, *6*, 180.
[16] L. J. Huo, J. H. Hou, H. Y. Chen, S. Q. Zhang, Y. Jiang, T. L. Chen, Y. Yang, *Macromolecules* **2009**, *42*, 6564.
[17] S. Loser, C. J. Bruns, H. Miyauchi, R. P. Ortiz, A. Facchetti, S. I. Stupp, T. J. Marks, *J. Am. Chem. Soc.* **2011**, *133*, 8142.
[18] H. J. Chen, Y. L. Guo, G. Yu, Y. Zhao, J. Zhang, D. Gao, H. T. Liu, Y. Q. Liu, *Adv. Mater.* **2012**, *24*, 4618.
[19] M. S. Chen, O. P. Lee, J. R. Niskala, A. T. Yiu, C. J. Tassone, K. Schmidt, P. M. Beaujuge, S. S. Onishi, M. F. Toney, A. Zettl, J. M. J. Fréchet, *J. Am. Chem. Soc.* **2013**, *135*, 19229.
[20] N. Blouin, A. Michaud, M. Leclerc, *Adv. Mater.* **2007**, *19*, 2295.
[21] J. R. Matthews, W. J. Niu, A. Tandia, A. L. Wallace, J. Y. Hu, W. Y. Lee, G. Giri, S. C. B. Mannsfeld, Y. T. Xie, S. C. Cai, H. H. Fong, Z. N. Bao, M. Q. He, *Chem. Mater.* **2013**, *25*, 782.
[22] A. T. Yiu, P. M. Beaujuge, O. P. Lee, C. H. Woo, M. F. Toney, J. M. J. Frechet, *J. Am. Chem. Soc.* **2012**, *134*, 2180.
[23] Z. Li, Y. G. Zhang, S. W. Tsang, X. M. Du, J. Y. Zhou, Y. Tao, J. F. Ding, *J. Phys. Chem. C* **2011**, *115*, 18002.
[24] J. Lee, A. R. Han, H. Yu, T. J. Shin, C. Yang, J. H. Oh, *J. Am. Chem. Soc.* **2013**, *135*, 9540.
[25] I. Kang, H. J. Yun, D. S. Chung, S. K. Kwon, Y. H. Kim, *J. Am. Chem. Soc.* **2013**, *135*, 14896.
[26] J. Lee, A. R. Han, J. Kim, Y. Kim, J. H. Oh, C. Yang, *J. Am. Chem. Soc.* **2012**, *134*, 20713.
[27] L. Meager, R. S. Ashraf, S. Mollinger, B. C. Schroeder, H. Bronstein, D. Beatrup, M. S. Vezie, T. Kirchartz, A. Salleo, J. Nelson, L. McCulloch, *J. Am. Chem. Soc.* **2013**, *135*, 11537.
[28] Y. H. Lee, A. Ohta, Y. Yamamoto, Y. Komatsu, K. Kato, T. Shimizu, H. Shinoda, S. Hayami, *Polyhedron* **2011**, *30*, 3001.
[29] H. Bronstein, Z. Y. Chen, R. S. Ashraf, W. M. Zhang, J. P. Du, J. R. Durrant, P. S. Tuladhar, K. Song, S. E. Watkins, Y. Geerts, M. M. Wienk, R. A. J. Janssen, T. Anthopoulos, H. Sirringhaus, M. Heeney, I. McCulloch, *J. Am. Chem. Soc.* **2011**, *133*, 3272.
[30] M. Shahid, T. McCarthy-Ward, J. Labram, S. Rossbauer, E. B. Domingo, S. E. Watkins, N. Stingelin, T. D. Anthopoulos, M. Heeney, *Chem. Sci.* **2012**, *3*, 181.
[31] R. J. Kline, M. D. McGehee, E. N. Kadnikova, J. S. Liu, J. M. J. Frechet, *Adv. Mater.* **2003**, *15*, 1519.
[32] R. Noriega, J. Rivnay, K. Vandewal, F. P. V. Koch, N. Stingelin, P. Smith, M. F. Toney, A. Salleo, *Nat. Mater.* **2013**, *12*, 1037.
[33] C. M. Cardona, W. Li, A. E. Kaifer, D. Stockdale, G. C. Bazan, *Adv. Mater.* **2011**, *23*, 2367.
[34] A. L. Dyer, E. J. Thompson, J. R. Reynolds, *ACS Appl Mater Inter* **2011**, *3*, 1787.
[35] J. L. Bredas, J. E. Norton, J. Cornil, V. Coropceanu, *Acc. Chem. Res.* **2009**, *42*, 1691.
[36] S. R. Forrest, *Nature* **2004**, *428*, 911.
[37] H. C. Yang, T. J. Shin, L. Yang, K. Cho, C. Y. Ryu, Z. N. Bao, *Adv. Funct. Mater.* **2005**, *15*, 671.
[38] A. R. Aiyar, J. I. Hong, R. Nambiar, D. M. Collard, E. Reichmanis, *Adv. Funct. Mater.* **2011**, *21*, 2652.
[39] I. Mcculloch, M. Heeney, C. Bailey, K. Genevicius, I. Macdonald, M. Shkunov, D. Sparrowe, S. Tierney, R. Wagner, W. M. Zhang, M. L. Chabinyc, R. J. Kline, M. D. Mcgehee, M. F. Toney, *Nat. Mater.* **2006**, *5*, 328.
[40] R. J. Kline, M. D. Mcgehee, M. F. Toney, *Nat. Mater.* **2006**, *5*, 222.
[41] Y. D. Park, J. K. Park, J. H. Seo, J. D. Yuen, W. H. Lee, K. Cho, G. C. Bazan, *Adv. Energy Mater.* **2011**, *1*, 63.